Competition between chaos and order: Mixing and segregation in a spherical tumbler

J. F. Gilchrist and J. M. Ottino
Department of Chemical Engineering, Northwestern University, Evanston, Illinois 60208, USA
(Received 7 July 2003; published 24 December 2003)

We investigate the competition between granular mixing and segregation in a sphere rotating and rocking on two orthogonal axes. Operation corresponds to the continuous-flow regime and the flow within the sphere is three-dimensional and time-periodic. Experimental results are organized in a frequency/amplitude phase diagram showing modes of segregation (band formation/no axial bands); segregated bands are remarkably robust and survive rocking amplitudes as large as 60 degrees over a wide range of frequencies. Details differ, but the phenomenon occurs under both dry and slurry conditions, that is, when all air is replaced by a liquid. Experimental space-time plots of the stationary segregated patterns agree well with Poincaré maps obtained using a continuum model of the flow, suggesting that the final segregation patterns are relatively independent of materials tumbled.

DOI: 10.1103/PhysRevE.68.061303 PACS number(s): 45.70.Mg, 45.70.Qj

I. INTRODUCTION

Much fundamental research has been carried out in the field of granular material in the past few years and significant progress has been made [1,2]. However, several important questions remain. Foremost among these is the development of theory to describe mixing in three-dimensional (3D) flows; another is segregation and its interplay with mixing. It is well known that the flow of binary mixtures of granular materials almost invariably leads to unmixing or segregation. The effect is triggered by differences in particles' size (*S* systems) or density (*D* systems). Segregation is crucially important in many industries and natural processes, however we are far from being able to predict segregation patterns in simple systems with 3D flow.

A few manifestations of mixing and segregation, such as radial and axial segregation, have become prototypical and studied extensively [3]. In most of the studies of radial segregation, the flow is quasi-2D; in axial segregation the flow is primarily 2D in the cross section of the cylinder with a much weaker axial flow set by the segregation itself. For instance, Zik *et al.* [4] studied axial segregation in containers with periodically modulated walls; the regime considered was discrete avalanches. These authors observed that smaller beads form bands in the ''bellies'' and large beads in the necks. Unquestionably the prevalent flows in practice are 3D flows. However, there are few fundamental studies of mixing and segregation corresponding to full 3D flows. Knowledge is fragmentary. Experiments involving mixing and rocking of cylinders suggest that rocking is an effective mechanism to enhance mixing [5]. However, this hypothesis has not been tested thoroughly.

Here we present a study of mixing and segregation in a spherical tumbler capable of undergoing independent programmed motions in two orthogonal directions (Fig. 1). The spherical geometry presents a clear advantage from a theoretical viewpoint: the boundary between the granular media and air is always a circle regardless of the forcing (we assume that the forcing is such that the interface remains flat, that is, the system operates in the continuous-flow regime; our experiments correspond to this regime as well).

The preferred mode of segregation in a rotated sphere is a single axial band. In an attempt to understand the perturbations necessary to break axial bands, we found that banding is surprisingly robust, surviving rocking amplitudes as high as 60 degrees. We demonstrate that the existence of various segregation patterns in the rocking sphere is a direct result of the stability of the underlying flow. These patterns align with invariant regions of the flow as predicted by a simple continuum model that describes advection in the absence of diffusion and segregation. This report is structured as follows. Section II describes the experimental method, and computational aspects are described in Sec. III. The results are presented in Sec. IV; a subsection in Sec. IV describes preliminary results for slurries. Following a discussion in Sec. V, our conclusions are summarized in Sec. VI.

II. EXPERIMENTAL METHODS

The experimental apparatus used in this study consists of a clear acrylic spherical container with radius $R=70$ mm held and rotated on one axis ($A1$) and capable of undergoing rocking about an orthogonal axis ($A2$) [see Fig. 1(a)]. In the dry experiments reported here, the tumbler is half full with glass beads (Quackenbush), $\frac{1}{3}$ of which are 0.8 mm (fluorescent) and $\frac{2}{3}$ are 2.0 mm (black) diam, respectively. We have also performed experiments with different dry granular mixtures, bead ratios, and tumblers sizes and found that the results presented here are also generally represented in these other cases. A few caveats should be mentioned as well. These results focus on a half-full sphere. It is clear, based on results obtained in cylinders and quasi-2D geometries, that changing the fill level can lead to unmixed invariant regions. The effects of filling, however, are not considered here. We also report a few representative results of experiments conducted under slurry conditions, where all the air in the container is replaced by either water or a 67% NaI solution. These systems consist of particles differing in both size and density.

Figures 1(b) and 1(c) illustrate the rotation protocol and coordinate system. Axes $A1$ and $A2$ are rotated using computer-driven stepper motors (Compumotor). The first

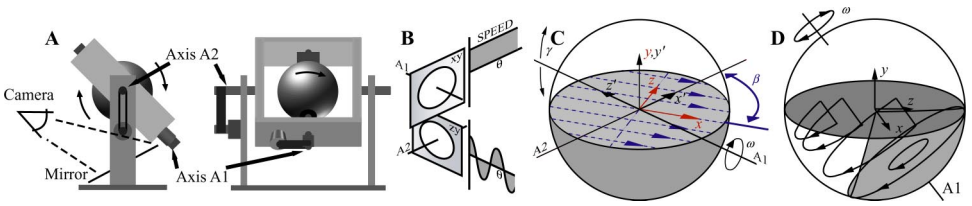

FIG. 1. (Color online) Apparatus, rocking protocol, and coordinate system. (a) Two independent axes, $A1$ and $A2$, rotate a spherical tumbler. (b) Depiction of the rocking protocol; the sphere rotates about $A1$ at constant angular velocity and about $A2$ sinusoidally. (c) Coordinates relative to the flow (red) and to the lab (black). γ is the instantaneous rocking angle and β is the angle between the direction of flow and $A2$. Streamlines in different directions cross at different times, producing chaotic advection within the mixer. (d) When the mixer is rotating on an angle, a region exists where streamlines do not intersect the free surface and material rotates as a solid body without mixing.

motor rotates the sphere on $A1$ at a constant angular velocity. The second produces sinusoidal motion on $A2$, where the rocking angle is defined as $\gamma = A\sin(2\pi\phi t)$. Rocking is scaled by the constant angular velocity on $A1$, $f = \phi/\omega$ and $t = \theta/(2\pi\omega)$, such that $\gamma = A\sin(f\theta)$. This simplifies the relationship between rocking and rotation. For $f = 1$, one rocking cycle is completed after one full rotation on $A1$. The amount of rotation on $A1$ is denoted θ; thus $\theta = 2\pi/f$ corresponds to one full cycle. This scaling is such that at $f = 1$ one rocking cycle occurs for every full revolution on $A1$. The parameters ω, A, and f are chosen such that the flow is always in the continuous-flow regime where the free surface is flat and free of instabilities ($\omega = 5$ rpm dry, $\omega = 3$ rpm under slurry conditions; $0.2 < f < 2$ and $0 \leqslant A \leqslant 70°$). The same general phenomena presented here occur for different rotation rates within the rolling regime.

A typical experiment starts with the material initially well mixed. This is accomplished (approximately) by using erratic tumbler motions. It is manifestly impossible to produce *exactly* the same initial condition twice. Therefore, every experiment is repeated at least twice—and as many as 20 times. All reported results are robust. The main limitation of all the experiments reported here is that we are able to report only what occurs at the boundary of the tumbler. Images of the bottom of the tumbler are taken at the end of a cycle when $A1$ is horizontal ($\gamma = 0$). Ultraviolet (uv) light is used to illuminate the fluorescent beads and glare is reduced using a uv filter in order to identify the segregated domains.

III. COMPUTATIONS

Experimental studies in tumblers indicate that flow occurs on a ''fixed bed'' that deforms plastically with a velocity decaying exponentially with distance into the bed [6–8]. Here we extend the continuum model presented in Khakhar *et al.* [9], which has been extensively tested in 2D tumbling and 2D heap formation [10]. The model presented below does not include segregation (how to include segregation is indicated in [11]) and thus, strictly speaking, it applies only to one-phase systems. While it is clear a more complicated model is necessary to describe the transient behavior of segregation, we assume that this model also applies to systems that behave as one-phase systems once the segregation processes have reached a steady state. The reason for this assumption is discussed in the Conclusions.

Coordinates are based on the free surface of the material, which is assumed flat [Fig. 1(c)]. The x axis always points in the flow direction, which changes as a function of time, the y axis is normal to the free surface, and the z axis is orthogonal to the x–y plane (the origin is at the center of the sphere). The instantaneous surface velocity at the fluid-granular media interface is proportional to the flow distance, i.e., $L = R\sqrt{1-(z/R)^2}$ and δ_0 is the thickness of the layer at $x = 0$, $z = 0$, proportional to L ($\delta_0 = 0.05R$ is estimated from 2D experiments) [12]. The flow region is restricted to a thin lenslike region of form $\delta = \delta_0 L[1-(x/L)^2]$ and the region below this surface represents material in solid body rotation. From here on, variables are dimensionless where spatial variables are scaled with R and time with $1/\omega$. The instantaneous direction of the flow in the surface depends on the position of the surface with respect to the direction of gravity. Lab-frame coordinates are defined as x' (projection of $A2$), y' (opposite to gravity), and z'. The instantaneous angle between x and x', β, defines the direction of the flow and is given by $\beta = \tan^{-1}[(d\gamma/d\theta)/\cos(\gamma)]$. The equations for velocity in the flowing layer for a simple linear shear are

$$v_x = 2uLM\left(1+\frac{y}{\delta}\right), \tag{1}$$

$$v_y = -Mx\left(\frac{y}{\delta}\right)^2. \tag{2}$$

Here, $u = 1/(2\delta_0)$ is the average velocity at $x = 0$, $z = 0$. The function M in Eqs. (1) and (2) is obtained using a mass balance of material in and out of the flowing layer due to rocking,

$$M = \sqrt{\cos^2(\gamma)+\left(\frac{d\gamma}{d\theta}\right)^2}. \tag{3}$$

A few general observations are in order. An examination of the kinematics of the flow within the sphere shows that most streamlines produced by solid body rotation intersect the flowing layer. However, a cone-shaped stream surface exists where material within circulates without intersecting the surface layer flow [Fig. 1(d)]. The size of this region depends on γ, and all streamlines intersect the flowing layer when $\gamma = 0$. Particle paths (and Poincaré plots) are computed by integrating $dx/dt = v_x$ and $dy/dt = v_y$ with $x = X$ and $y = Y$ at $t = 0$. As is standard in this type of calculations, col-

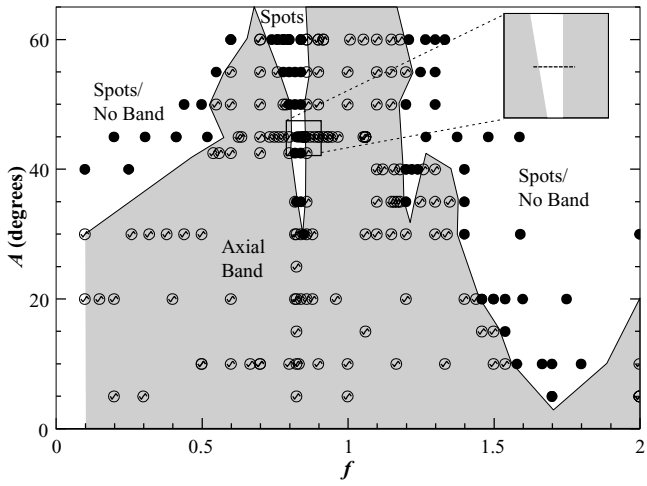

FIG. 2. Experimental phase diagram with "Arnold tongues." The gray region roughly outlines where axial banding occurs. Stability of a band is surprisingly sensitive to the frequency and amplitude. Note regions of spots growing upward from (f,A) of (0.85, 30°), (1.2, 30°), and (1.7, 5°) corresponding roughly to ratios of 1:2, 1:3, and 1:4.

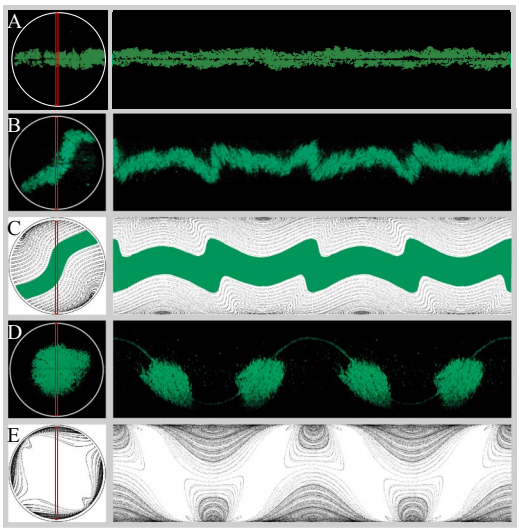

FIG. 3. (Color online) Bottom view of experimental (A,B,D) and computer-generated (C,E) space-time plots of bands and spots. Left are static pictures and right are spatio-temporal composites of the same experiment where a vertical line of pixels (represented by a red line) is selected from each frame of consecutive pictures. Picture (a) corresponds to the system without rocking. Values of (f,A) are (b) (1.0, 45°), (c) (1.0, 45°), (d) (0.842, 45°), and (e) (0.957, 45°). In (c), the center trajectories are shaded for clarity.

lisional diffusion is not included. We remark that different functional forms of the velocity field. [Eqs. (1) and (2)], for example $v_x \sim y^{3/2}$, $v_y \sim xy^{5/2}$, and different functionalities for the layer profile, e.g., $\delta = \delta_0 \sqrt{1-(x/L)^2}$, give essentially the same results, indicating that global aspects (i.e., the shape of the container and forcing) control the important details of the physics.

This model applies to any prescribed motion about $A2$. One can consider the proposed sinusoidal rocking as a perturbation to a base case, rotation without rocking, where $A1$ is always horizontal and each cross section is a simple circle. When A and f are nonzero, there is an axial component of the flow. Large values of A and f produce flows that are almost perpendicular to the x' direction.

IV. OBSERVED PATTERNS

A. General observations

Consider the dry system described above. Results are summarized in phase diagram in terms of the forcing parameters A and f (Fig. 2). All sets of parameters leading to a fully connected surface band are represented as ✓. At certain parameters, a band does not wrap continuously around the granular bed; these may be spots or simply no observable pattern at the boundaries. These points are represented as •. The diagram contains at total of 227 data points, each point repeated between 2 and 20 times, with most of the repetition taking place for points near the separation between domains. In these regions, we estimate that the standard deviation of the location of the boundaries is smaller than the size of the circles.

The phase space diagram shows that axial bands are stable for a wide range of frequencies and amplitudes (the gray region in Fig. 2). Rotation on a single axis $(A=0°)$ produces a stable single band in the center of the sphere after ~5 min of rotation at 5 rpm [Fig. 3(a)]. In Fig. 3, we present the view of the bottom of the container as both single still pictures and spatio-temporal pictures produced by extracting the center pixels along a vertical line of each frame of digital video. From this perspective, the bottom of the container rotates to the left. This combination of materials in this container never produces more than one band. We found that different materials produce multiple bands that eventually coarsen into a single band. This band in the middle of the sphere is analogous to each band of smaller beads found in the "bellies" of the axial container studied by Zik *et al.* [4] We focus primarily on the long-time segregation pattern. The sinusoidal curve seen, for example, in Fig. 3(d) is the seam of the container adjoining the two hemispherical halves, demonstrating both the smoothness of rocking/rotation forcing and the continuity of the imaging. In a few cases, experiments have been conducted for up to 500 cycles.

At low A, 0°–10°, axial bands exist for most frequencies of rocking. An axial band wraps around the bottom of the granular bed and connects through the flowing layer [Fig. 3(b)]. Surprisingly, at certain frequencies, *bands are stable even when rocking angles are greater than* 60°. For different parameters, the band may be very wavy or relatively straight, however within the flowing layer it always aligns roughly in the direction of flow. Also, this band is often observed close to the center of the flowing layer at all times (in the frame of the flowing layer where flow is in the x direction, it is located at or near $z=0$). The final pattern begins to emerge after ~20 cycles, roughly the same amount of time as without rocking. The band may only contain smaller beads or have both small and large beads (denoted as "diffuse").

With increasing amplitude, there is an ''Arnold tongue''-like region [13] originating from $(f,A)=(0.85,30°)$ where the axially segregated band bifurcates into spots. Another tongue-like region is present at 0.85*(3/2) and yet another at 0.85*2. When spots form, the regions may also be well segregated with relatively sharp boundaries or diffuse ones. The spots are typically round, but in some cases they are V-shaped or four-pointed stars. Typically, they are only seen from the bottom (i.e., they only pass through the flowing layer) twice in each rocking cycle. It is difficult to capture images of these spots when they are located at either end of the tumbler and not at the bottom of the container. We should point out that high A and f ($f>2$ and $A>30°$) leads to the *cascading* regime and that the free surface becomes S-shaped when $\gamma\approx 0$. Also, high rocking angles ($A>75°$) lead to the avalanching regime when $d\gamma/d\theta\approx 0$. At some frequencies, there is no observable segregation pattern at the boundaries of the container; all small beads segregate to the center of the granular bed. All observed patterns produced from sinusoidal rocking have a translation/rotation symmetry such that each half-cycle has the same pattern as the previous half-cycle rotated 180° in the x'-z' plane.

B. Underlying mixing

The flow is 3D and time-periodic, making visualization difficult. In order to capture the quasiperiodic trajectories, we define a surface Poincaré map as follows. Consider a number of points close to the bounding surface of the container ($r=0.95$), then convect the points for 200 cycles and plot their locations at the end of each cycle. As points pass through the flowing layer, they return to the same hemispherical surface. Chaotic trajectories typically stay close, but are not bound to this surface. This reduces the picture roughly to two dimensions, the physical analogy being similar to capturing the structure in layers, as in the peeling of an onion. Figures 3(c) and 3(e) show bottom views of this hemisphere constructed in the above manner. Spatio-temporal pictures, constructed using the midsection of the Poincaré plots, as indicated in Fig. 3, capture the dynamics of the map over one entire cycle.

The behavior of the simulated system in the amplitude-frequency plane is rich. Examples are shown in Figs. 3(c), 3(e), 4(b), and 5(e). At low amplitude (A) and low frequency (f), quasiperiodic trajectories are prevalent. At high A and high f, essentially all particle trajectories are chaotic with a very small amount of trajectories trapped within regular regions—areas of poor mixing located around elliptical periodic points. The behavior between these two states is complex. At certain parameters, elliptic (centers of regular regions) or hyperbolic periodic points (regions of high stretching) dominate mixing. Even at high A, there are frequencies where quasiperiodic orbits exist in the middle of the sphere, suggesting material transport between hemispheres is weak. All maps show 180° rotational symmetry.

C. Bifurcation from a band to spots

Consider now the narrow range of frequencies in the phase diagram where the band bifurcates into spots and back into bands (the magnified region of Fig. 2). In Fig. 4, this bifurcation is investigated closer by creating successive spatio-temporal plots of the patterns at frequencies $0.824\leqslant f\leqslant 0.856$. The band appears to ''pinch-off'' at distinct times in the rocking cycle. After pinch-off, the spots contract. At yet slightly higher frequencies, the spots stretch out back into bands. Interestingly, these spots are at the same location within the cycle where the bands originally pinched-off at lower frequencies. Graphing the intensity of smaller beads throughout a cycle demonstrates this phase shift [Fig. 4(c)]. The bands initially break in the cycle when $\gamma=0$. The spots, originally located at $d\gamma/d\theta=0$, migrate to this part of the cycle when $\gamma=0$. It should be noted that this pinch-off is *not*

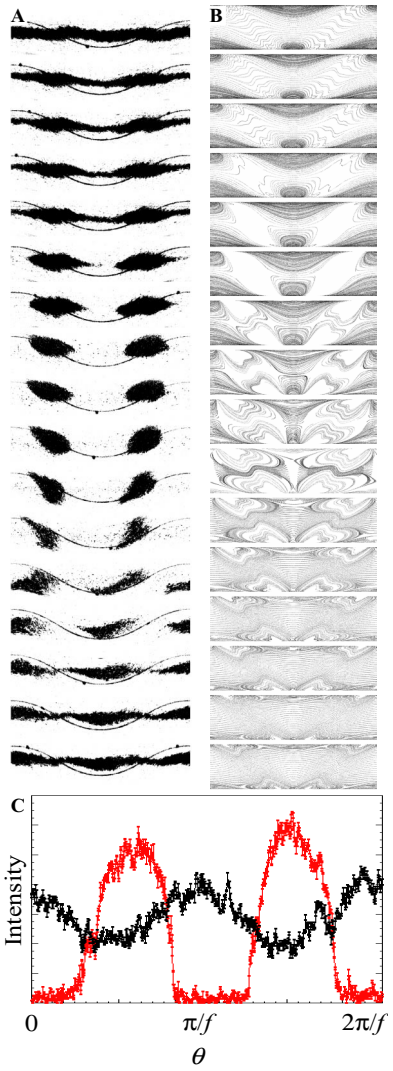

FIG. 4. (Color online) Band to spots and back to bands. Experimental space-time plots (a) show a clear bifurcation over a narrow range of frequencies ($0.824\leqslant f\leqslant 0.856$) as does the Poincaré space-time plots [(b), $0.953<f<0.968$]. The computations show quasiperiodic trajectories that are disrupted by the emergence of two hyperbolic points that separate and merge with neighboring points. (c) the intensity of the topmost experimental space-time plot (black) and spots (gray, $f=0.852$) demonstrates the phase shift during this bifurcation.

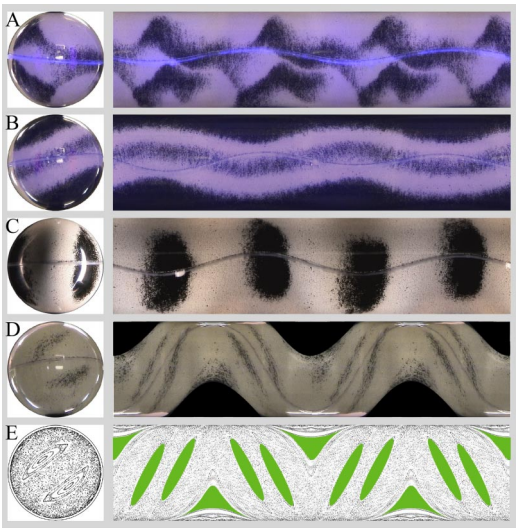

FIG. 5. (Color online) Various patterns in slurries. Space-time plots of axial segregation and spot formation in slurries [(a) (1.17, 10°), (b) (1.5, 10°), (c) (1.67, 10°), (d) (1.33, 40°)], and a computation exhibiting the same symmetries [(e) (1.5, 40°)]. In (d), regions where the frame of the apparatus rotates into view are blacked out.

a dynamic process, as each of these pictures is the *final* segregation pattern after many rocking cycles in separate experiments.

Computations—placed alongside the experimental pictures in Fig. 4—exhibit similar phenomena over a narrow range of frequencies and mimic the phase shift seen in the experiments. The quasiperiodic trajectories become wavy, dilating at one point in the cycle and necking at another. At a specific frequency, two hyperbolic points exist in the region where trajectories are dilating. These points drift apart as the frequency increases. Because of the periodicity of the flow, as a pair of hyperbolic points drifts apart, one approaches the hyperbolic point associated with the previous cycle and the other approaches a hyperbolic point associated with the next cycle. The hyperbolic points in each new pairing converge. They eventually annihilate each other, creating a part of the flow where quasiperiodic trajectories once again exist in the center of the map. These quasiperiodic trajectories once again have regions where they diverge and contract as seen at frequencies lower than the bifurcation, however the regions have an apparent phase shift of 90° compared to pictures at lower frequencies, as is seen in experiments.

D. Slurry-condition experiments

A similar picture to the one described above occurs when the system is run under slurry conditions, i.e., when air is replaced by a liquid, completely filling the container (four representative results, using water as the working fluid, are shown in Fig. 5). These results are obtained using a granular mixture with particles differing in both size and density (0.2 mm glass and 0.8 mm zirconium silicate). This mixture segregates remarkably fast in conventional axial segregation experiments in long cylinders. Figures 5(d) and 5(e) show the agreement between the experiments and the model, which, we stress, completely ignores the presence of the fluid.

Several experiments were carried out using as a fluid a solution of NaI, in order to visualize the internal structure of the segregated structures as reported in [14] (a saturated solution of NaI at room temperature roughly matches the refractive index of glass). The visualization of internal structures, however, is difficult. A few salient points, the result of a large number of experiments, are summarized here. In general, the same general behavior seen in the dry case is found in slurries, therefore we focus primarily on the differences with respect to the dry case. More bands (as many as five bands of smaller beads) may appear. Moreover, these bans appear faster than in the corresponding dry system (in about 10 rotations; this is consistent with the observations in [11]). Over time they coarsen into one or two bands. For instance, in Fig. 5(a), a single band splits into two, where one ends and the other continues to wrap around the granular bed. We have also observed reverse axial banding [small beads at the ends in Fig. 5(b)]. We conjecture from a few repeated experiments that this may depend on initial conditions. In general terms, the stability of banding in the presence of rocking is qualitatively similar to the dry case. Spots are stable at certain frequencies and amplitudes, and as in the dry case, show only two spots per cycle [Fig. 5(c)]. However, we have observed up to six spots per cycle [Fig. 5(d)] corresponding to period 6 regular regions found computations [Fig. 5(e)].

V. DISCUSSION

Axial banding is robust. When material parameters are such that axial segregation occurs, bands are hard to destroy. Axial bands are found at surprisingly high rocking amplitudes, and their stability is sensitive to rocking frequency. At the same time, it is evident that there is a rough correspondence in final segregation pattern between the model and the experimental results. This happens seemingly independent of material parameters, even though the dry *S* systems considered in our experiments are, in general, significantly more taxing from a modeling standpoint than the corresponding *D* systems. The reason for the additional complexity is as follows. In *S* systems, in conditions occurring typically when the container is slightly more that half filled, the flowing layer may alternate between nearly 100% small particles and 100% large particles. Thus, depending on the composition of the layer, the flow may become time-periodic under *steady rotation* leading to segregated structures that resemble the spokes of a wheel [7]. No such thing happens in *D* flows; the flow in the layer is (nearly) steady and no additional time periodicity arises due to composition. This difference between *S* and *D* systems is clearly evident in the 2D experiments reported in [8]. Under such conditions, the present model does not apply and significant changes are necessary.

It is clear, however, that our model works well. This may appear unexpected, as the model does not contain segregation. Therefore, how can we then rationalize the agreement between experiments and computations? There are two parts to the explanation. (i) If no significant time effects arise from the flow composition in the layer, the system, once in steady

state, behaves essentially as a single fluid and can be modeled as such. (ii) Segregated regions are invariant regions, i.e., segregated domains are mapped onto themselves. Unlike immiscible fluids, one may argue that the boundary between two phases has no surface tension; stresses and velocities are continuous across the interface. Segregation, once completed, has to follow the template provided by the Poincaré map. It is also obvious that the only place where segregation occurs is in the layer itself; it is the only place with nonzero shear rates. In fact, the layer is the only point of entry of materials into segregated domains.

The Arnold tongues observed at $f=0.85$ and rational multiples of this frequency suggest that frequency locking may be responsible for the organization of bands and spots. However, the model does not directly predict frequency-locking, as suggested by the experimental phase diagram. Bifurcations in the surface Poincaré maps are created via period-doubling. Like frequency-locking, periodic points exist in the map when the frequencies associated with rocking and circulation are commensurate. A may be interpreted as the magnitude of the nonlinear terms, and increasing A increases the range of frequencies where periodic points exist.

We also conducted several experiments using cubes and using biaxial motions of the axes (where both axes undergo the same protocol). A full account of the results will be given elsewhere. Given the substantial difference in the dynamics of axial segregation in long cylinders with circular and square sections [15], we expect very different behavior with respect to the sphere, and this is indeed the case. However, one general observation should be made. We stated earlier the reasons for the rough agreement between experiments and computations in the sphere. A similar comment applies here: The final structure of the segregated regions in the cube, though not the dynamics, can be largely predicted by the continuum model without invoking segregation. Conversely, this also suggests that an observed segregation pattern can give insight into the structure of the underlying flow.

VI. CONCLUSIONS

In novel experiments in a rotating-rocking sphere, stable axial bands are found at surprisingly high rocking amplitudes, and their stability is sensitive to rocking frequency. We constructed a phase diagram showing when axial bands and spots are stable. A simple continuum model of the underlying 3D time-periodic flow predicts the general shape of the phase diagram, along with the shape and stability of segregated patterns in systems with different bead sizes, densities, and interstitial fluids. This pattern formation is largely independent of the material parameters. Based on these observations, predictions of mixing and segregation in more complex geometries may not necessarily depend on understanding the underlying mechanisms of segregation.

ACKNOWLEDGMENTS

We are grateful for discussions with Devang Khakhar, Rich Lueptow, and Paul Umbanhowar. This research was supported by DOE, Office of Basic Energy Sciences.

[1] H.M. Jaeger, S.R. Nagel, and R.P. Behringer, Rev. Mod. Phys. **68**, 1259 (1996).
[2] J. Duran, *Sands, Powders and Grains. An Introduction to the Physics of Granular Materials* (Springer-Verlag, New York, 2000).
[3] G.H. Ristow, *Pattern Formation in Granular Materials* (Springer, New York, 2000).
[4] O. Zik, D. Levine, S.G. Lipson, S. Shtrikman, and J. Stavans, Phys. Rev. Lett. **73**, 644 (1994).
[5] C. Wightman and F.J. Muzzio, Powder Technol. **98**, 125 (1998).
[6] D. Bonamy, F. Daviaud, and L. Laurent, Phys. Fluids **14**, 1666 (2002).
[7] T.S. Komatsu, S. Inagaki, N. Nakagawa, and S. Nasuno, Phys. Rev. Lett. **86**, 1757 (2001).
[8] N. Jain, J.M. Ottino, and R.M. Lueptow, Phys. Fluids **14**, 572 (2002).
[9] D.V. Khakhar, J.J. McCarthy, T. Shinbrot, and J.M. Ottino, Phys. Fluids **9**, 31 (1997).
[10] D.V. Khakhar, A.V. Orpe, P. Andresén, and J.M. Ottino, J. Fluid Mech. **441**, 255 (2001).
[11] K.M. Hill, D.V. Khakhar, J.F. Gilchrist, J.J. McCarthy, and J.M. Ottino, Proc. Natl. Acad. Sci. U.S.A. **96**, 11701 (1999).
[12] D.V. Khakhar, J.J. McCarthy, J.F. Gilchrist, and J.M. Ottino, Chaos **9**, 195 (1999).
[13] G.L. Baker and J.P. Gollub, *Chaotic Dynamics* (Cambridge Univ. Press, Cambridge, UK, 1999), pp. 93–94.
[14] N. Jain, D.V. Khakhar, and J.M. Ottino, Phys. Rev. Lett. **86**, 3771 (2001).
[15] K.M. Hill, N. Jain, and J.M. Ottino, Phys. Rev. E **64**, 011302 (2001).